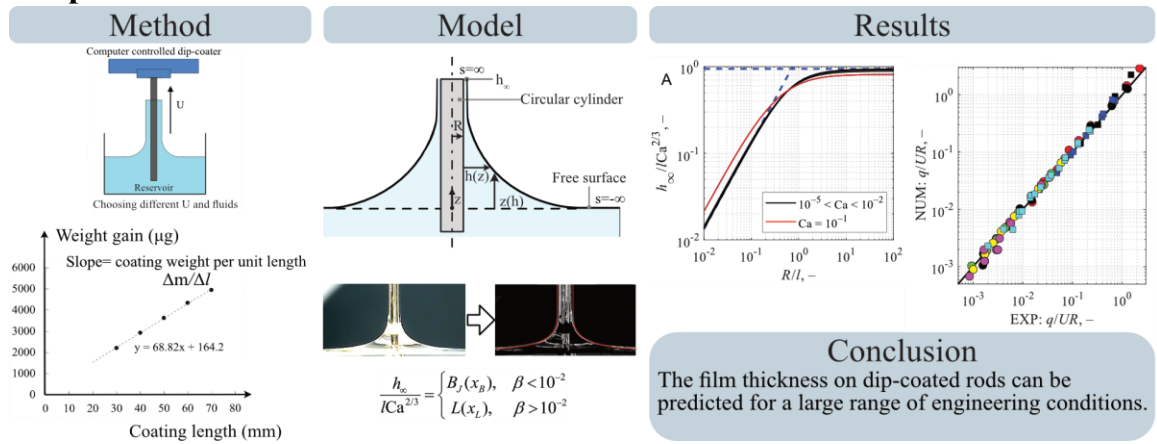
1 Graphical abstract.



Dip coating of cylinders with Newtonian fluids

- Zhao Zhang^a, Arthur Salamatin^{b,c}, Fei Peng^{a,d}, Konstantin G Kornev^{a,d*}
- ^a Department of Materials Science and Engineering, Clemson University, Clemson, SC
- 6 29634

2

3

4

5

- 7 b Institute of Mechanics and Engineering, FRC Kazan Scientific Center, Russian
- 8 Academy of Sciences, Russian Academy of Sciences, 2/31 Lobachevsky str, Kazan,
- 9 420111, Russia
- 10 ^c Institute of Geology and Petroleum Technologies & Institute of Computational
- 11 Mathematics and Information Technologies, Kazan Federal University, Kazan, 420008,
- 12 Russia

15

- 13 d Center for Optical Materials Science and Engineering Technologies
- 14 (COMSET), Clemson University, Anderson, SC, 29625

Abstract

- 16 Hypothesis: The Landau-Levich-Derjaguin (LLD) theory is widely applied to predict the
- 17 film thickness in the dip-coating process. However, the theory was designed only for flat
- plates and thin fibers. Fifty years ago, White and Tallmadge attempted to generalize the
- 19 LLD theory to thick rods using a numerical solution for a static meniscus and the LLD
- 20 theory to forcedly match their numeric solution with the LLD asymptotics. The White-
- 21 Talmadge solution has been criticized for not being rigorous yet widely used in engineering

- 22 applications mostly owing to the lack of alternative solutions. A new set of experiments
- 23 significantly expanding the range of White-Tallmadge conditions showed that their theory
- 24 cannot explain the experimental results. We then hypothesized that the results of LLD
- 25 theory can be improved by restoring the non-linear meniscus curvature in the equation.
- With this modification, the obtained equation should be able to describe static menisci on
- any cylindrical rods and the film profiles observed at non-zero rod velocity.
- 28 Experiment: To test the hypothesis, we distinguished capillary forces from viscous forces
- by running experiments with different rods and at different withdrawal velocities and video
- tracking the menisci profiles and measuring the weight of deposited films. The values of
- 31 film thickness were then fitted with a mathematical model based on the modified LLD
- 32 equation. We also fitted the meniscus profiles.
- 33 Findings: The results show that the derived equation allows one to reproduce the results of
- 34 the LLD theory and go far beyond those to include rods of different radii. A new set of
- 35 experimental data together with the White-Tallmadge experimental data are explained with
- 36 the modified LLD theory. A set of simple formulas approximating numeric results have
- 37 been derived. These formulas can be used in engineering applications for the prediction of
- 38 the coating thickness.

40

41

42

43

44

45

46 47

48 49

50

51 52

53 54

55

56

57

58

59

Keywords

Dip coating; lubrication flow; Landau-Levich-Derjaguin (LLD) theory; capillarity,

1. Introduction

The dip coating process schematically shown in Fig. 1, is a popular technological process used in a variety of industrial fields [1]. An article of interest, say a cylinder in Fig. 1, is first immersed in a liquid reservoir and then is pulled out. As the substrate is moved upward, it picks up some liquid film. This film can be further cured to make a solid coating. In the case of deposition of solutions/dispersions/suspensions, the solvent evaporates, leaving behind a solid deposit of interest. Due to its simple process and ease of control, the dip coating is widely applied in industry and manufacturing [1].

It is used, for example, for making the energy-saving coating on architectural glasses [2, 3], the biocompatible coating on medical implants [4], and the electrothermal coating on micro-heaters [5]. Different substrates, such as plates, cylinders, fibers, and articles of more complex shapes, can be dip-coated with different liquids [1, 6-24]. Fibers deserve special attention because the deposited liquid films are subject to capillary action when the surface tension of the cylindrical film forces the liquid to move back to the reservoir [6-11, 25-40].

To tailor the electrical, mechanical, thermal, and chemical properties of coatings, it is always important to control the thickness of the coating films [10-12, 32, 41-45]. The importance of this technology called for the development of a theory, which after the

seminal works of Landau, Levich [46] and Derjaguin [47, 48], became one of the crown jewels of surface science, the Landau-Levich-Derjaguin (LLD) theory. As the technology progresses and new coating materials and articles are developed, the demand for an understanding of controlling means for new coatings remains high despite the great history of this methodology [23, 44, 45].

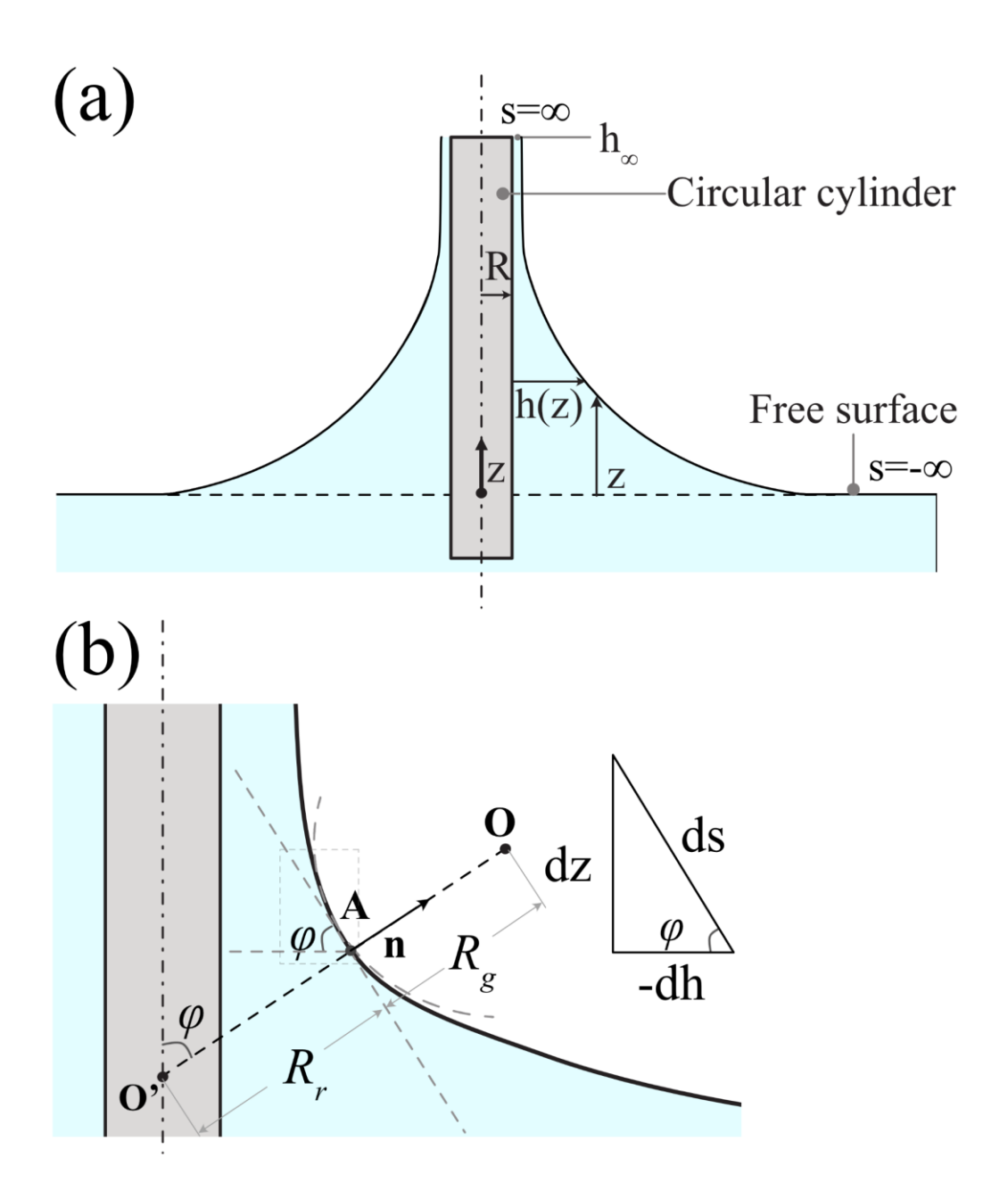


Fig. 1. (A) Schematic of the dip coating process. A circular cylinder of radius R is withdrawn vertically from a liquid reservoir at constant velocity U. z - is the cylinder axis, and R + h(z) is the meniscus profile – the generator curve. The film thickness h(z) increases from h_{∞} at $z \to \infty$ to $h \to \infty$ as one moves to the horizontal air-liquid interface, z = 0. In the film, the flow is assumed almost unidirectional and the film profile is shaped by the viscous, capillary, and gravitational forces. (B) Definition of two radii of curvatures of meniscus at an arbitrarily chosen point A on the film surface. An outward normal vector \mathbf{n} at point A is continued toward the air and from the liquid to make the straight line O'AO, where O' is the point of intersection of this line with the z-axis. This line makes angle φ with the z-axis. The quantity is called the inclination angle. Then the point O

on this line is the center of curvature and $|OA| = R_g$ is the radius of curvature of the generator curve – meniscus profile at point A. The distance $|O'A| = R_r$ is the second principal radius of curvature due to the rotation of this generator curve about the z-axis. Assuming that the arclength s increases with z while h – decreases, the differential of the arclength ds of this profile R + h(z)at point A is related to the differential dz as $dz = ds \sin \varphi$ and $\tan \varphi = -dz/dh$.

81

82

83

84 85

86

87

88 89

90

91

76

77

78

79

80

Landau and Levich [46] theoretically studied a dip coating process when a flat plate is steadily withdrawn vertically from the liquid reservoir of viscosity η and surface tension σ at low speed U. When the capillary number Ca = U $\eta/\sigma \ll 1$ is small, the flow does not significantly affect the shape of the meniscus formed on the plate. Landau and Levich subdivided the flow region onto three sub-regions: 1) the region of constant film thickness, $z \rightarrow \infty$; 2) the region of static meniscus; 3) and an intermediate transition region, which connects the region of constant thickness and the static meniscus, Fig. 1. The flow in the coating film influences the meniscus shape only in the transition region situated near the static contact line. This partitioning of the flow regions allowed Landau and Levich to successfully solve this non-linear free boundary problem of fluid mechanics to predict the thickness h_{∞} of a fluid film deposited on the plate:

92 93

94

95

99

100

101

102

103

106

107 108

109

$$h_{\infty} = A_{plate} \cdot l \cdot Ca^{\frac{2}{3}}, \qquad A_{plate} = 0.945, \quad Ca = U \eta/\sigma,$$
 (1)

where $l = \sqrt{\frac{\sigma}{g\rho_l}}$ is the capillary length, ρ_l is the density of the liquid, and g is the acceleration due to gravity. The capillary length gives an estimate of the height of the meniscus attached to a non-moving vertical plate. This Eq. (1) does not depend on any 96 97 plate dimensions, and hence the film thickness depends only on the physical properties of 98 fluids and velocity of the plate withdrawal.

However, when it comes to cylinders or fibers, the liquid-air interface becomes axisymmetric and is subject to the capillary compression in the radial direction [30, 47, 48]. Derjaguin and later White and Tallmadge recognized this fact and modified the Landau-Levich theory for thin fibers when the fiber radius R is small compared to the capillary length l ($R \ll l$) [30, 31, 47, 48]. The result is written as:

$$h_{\infty} = A_{fiber} \cdot R \cdot Ca^{\frac{2}{3}}, \qquad A_{fiber} = 1.34. \tag{2}$$

The striking difference with the plate case is that the film thickness becomes directly 104 proportional to the cylinder radius: the thinner the cylinder, the thinner the coating film! 105

There is no direct connection between Eq. (1) and Eq. (2), and it is not possible to predict what will happen with the deposited film when one increases the fiber radius. Intuitively, one expects that as R increases, the effect of meniscus curvature should become less critical and will not follow the case of a thin fiber. To study this problem, a dimensionless radius,

- 110 R/l, is naturally introduced. The coating scenario can now be divided into three cases [31]:
- 111 a) $R/l \gg 1$, when the cylinder radius is much greater than the height of meniscus attached
- to a plate made of the same material; b) $R/l \ll 1$, when the cylinder is much thinner than
- the height of meniscus attached to a plate made of the same material; c) R/l is close or
- comparable to 1, i.e., the cylinder diameter is comparable with the meniscus height.
- In the first case, there is a negligible curvature in the radial direction. Therefore, the coating
- scenario should be similar to the case of a flat plate, and the thickness can be predicted by
- Eq. (1), where the thickness is independent of the radius of the cylinder.
- In the second case, the thickness can be predicted by Eq. (2). A great deal of research has
- been performed to verify the dip-coating thickness in those two cases [1, 20, 29, 44, 48].
- However, when the ratio of the cylinder radius to the capillary length goes to 1, which is
- the case for many industrial applications with the cylinders of about 1 millimeter in
- diameter, such as an optical fiber or a metal wire, one requires additional experimental
- support for evaluation of the film thickness. This case has been studied by White and
- Tallmadge [31, 49]. As noticed by Wilson[50, 51] and further discussed in Refs.[1, 44],
- the White Tallmadge approach to accommodate gravity lacks mathematical rigor and
- hence cannot be used to predict the film thickness in a wide range of capillary numbers.
- 127 In this paper, we modify the LLD-model to include the full non-linear capillary pressure
- term in the equation for a film flow over a circular cylinder. This modification guarantees
- that the static meniscus is described exactly; thus the surface tension terms are correctly
- taken into account [50-52]. We numerically evaluate the effect of gravity and cylinder
- radius on the thickness of deposited films and verified theoretical results in experiments.
- 132 A large range of capillary numbers from 10^{-5} to 10^{-1} was covered. These data
- significantly enrich the set of results obtained by White and Tallmadge [31, 49] and
- confirm the predictions of the modified LLD model.

2. Materials and Methods

136137

138

2.1. Rods and liquids

- Stainless steel and brass rods with six different radii (R = 0.165mm, 0.202mm, 0.255mm,
- 140 1.15mm, 1.54mm, 2.35mm) were used in experiments. Before coating, all the rods were
- sonicated in an ultrasonic cleaner (VWR Ultrasonic Cleaner 97043-964, 35 kHz, 90 W) in
- acetone for 2 hours and dried thoroughly in ambient conditions. The used stainless steel
- and brass wires were smooth but unpolished. The spatial scale of the surface roughness is
- much smaller than the typical film thickness. The contact angles between the fluids and the
- high energy stainless steel and brass rods were very small, which can be verified in Fig. 6.
- 146 Thus, the fluids wetted the rods completely and hence adhesion between the fluids and the
- rod surfaces was strong. Thus, a macroscale description of the fluid flow in the film is

applicable where the nominal surface is assigned to have no-slip boundary condition for flow.

The dip coater (KSV NIMA Dip Coater) was used for coating the rods. The rod was attached to the dip coater holder by a clamp to ensure that the rod was fixed vertically. Then the rod was lowered into the fluid reservoir at a velocity of 100mm/min. After dipping to a certain targeted length, the rod was remained still for 15 seconds before withdrawing from the reservoir at a certain velocity. Five withdrawal velocities, 20mm/min, 50mm/min, 100mm/min, 200mm/min, and 500mm/min were chosen to adjust the capillary number. Purely viscous fluids such as glycerol (Fisher Scientific Inc.), hexadecane (Fisher Scientific Inc.), the standard viscosity oil Conostan S60 (SCP Science), and Sylgard 184 (Dow Corning), were used as the coating fluids; Sylgard 184 showed the Newtonian behavior up to the shear rate 18 s⁻¹ which are of interest to the dip coating conditions. The viscosity of the fluids was measured by a viscometer (Brookfield DV3THBCJ0). The density of the fluids was calculated by measuring the weight of fluid in a fixed volume liquid pycnometer (25ml) using an analytical balance (PI-214, Denver Instrument) at room temperature. The surface tension was measured by a Kruss DSA10 drop shape analysis system and analyzed by the DSA software. The dynamic menisci for a brass wire (R=0.202mm, R/l=0.13) drawn at different velocities (20 mm/min, 50 mm/min, 100 mm/min, 200 mm/min, 350mm/min, and 500 mm/min) out of a bath of Sylgard 184 were recorded by a Xcsource 20X-800X USB microscope camera.

All the properties were measured at 23°C. Based on the radii of rods and the capillary lengths, the dimensionless radii R/l were calculated for each group of experimental data and collected in Table 2.

171

148149

150151

152153

154155

156

157

158

159

160

161

162

163

164165

166

167

168

172 Table 1. Fluid Properties at Room Temperature (23°C)

Description of the fluid	Viscosity η $(mPa \cdot s)$	Density ρ_l (kg/m^3)	Surface tension σ (mN/m)	Capillary length, l (mm)
Sylgard 184	5100	1030	23.3	1.52
93 w% Glycerol- water mixture	270	1241	64.1	2.29
hexadecane	3.40	770	27.4	1.91
Conostan S60	102	869	30.9	1.91

174 Table 2 Cylinder Radii and Dimensionless Radii

Cylinder number	1	2	3	4	5	6
Material	Brass	Brass	Brass	Stainless	Stainless	Stainless
				steel	steel	steel
Radius (mm)	0.165	0.202	0.255	1.15	1.54	2.35
			Dime	nsionless rad	lius R/l	
Sylgard 184	0.11	0.13				
93 w% Glycerol-water mixture			0.11	-	-	-
Hexadecane			0.13	0.61	0.81	1.24
Conostan S60			_	0.61	0.81	1.24

2.2. The thickness of deposited film.

The following experimental protocol was developed to measure the coating thickness at the given experimental conditions. First, as shown in Fig. 2A, the rods were weighed by a semi-micro-balance (Sartorius LE 26D) before and after the dip-coating experiment when the rods were coated over five different lengths ($\lambda = 30$ mm, 40mm, 50mm, 60mm, 70mm). The mass of the rod m_{dry} was subtracted from the observed mass after the dip-coating process, $m_{wet}(\lambda)$, to determine the mass gain $m(\lambda) = m_{wet}(\lambda) - m_{dry}$. The mass gain is shown to be a linear function of λ : $m(\lambda) = \frac{\Delta m}{\Delta \lambda} \lambda + m_d$, where the first term is the mass of the liquid film and m_d is the mass of the drop observed at the bottom of the withdrawn rod as shown in Fig. 2B.

We did not observe any difference in the sizes of the end droplets for the rods submersed in the liquid reservoir at different depths. Thus, the weight gain per unit length, $\Delta m/\Delta \lambda$, is proportional to the flux thickness q/U and does not depend on λ . The ratio $\Delta m/\Delta \lambda$ can be calculated from the slope of the weight gain vs. immersion length plots [31], Fig. 2C. The uncertainty of the slope was evaluated by the LINEST function in Excel. The uncertainty is shown in Table S1 of Supplementary Information. The average flux-based thickness q/U was calculated based on the slope, liquid density ρ_l , and the radius R of the coated rod as shown below

195
$$\frac{q}{U} = \frac{Q}{2\pi RU} = \frac{Q \cdot \Delta t}{2\pi RU \cdot \Delta t} = \frac{\Delta V \cdot \rho_l}{2\pi R\lambda \cdot \rho_l} = \frac{1}{2\pi R} \cdot \frac{\Delta m}{\Delta \lambda} \cdot \frac{1}{\rho_l},$$
194 (3)

where Δt is the time of the rod withdrawal, $\Delta V = Q \cdot \Delta t$ is the volume of the deposited liquid, $\lambda = U \cdot \Delta t$ is the length of the coated part of the rod, Q is the total flux in the annular film. During the dip-coating process, the capillary number Ca varied from 3×10^{-5} to 7×10^{-1} by adjusting the withdrawal velocities and using different fluids, see Table 1.



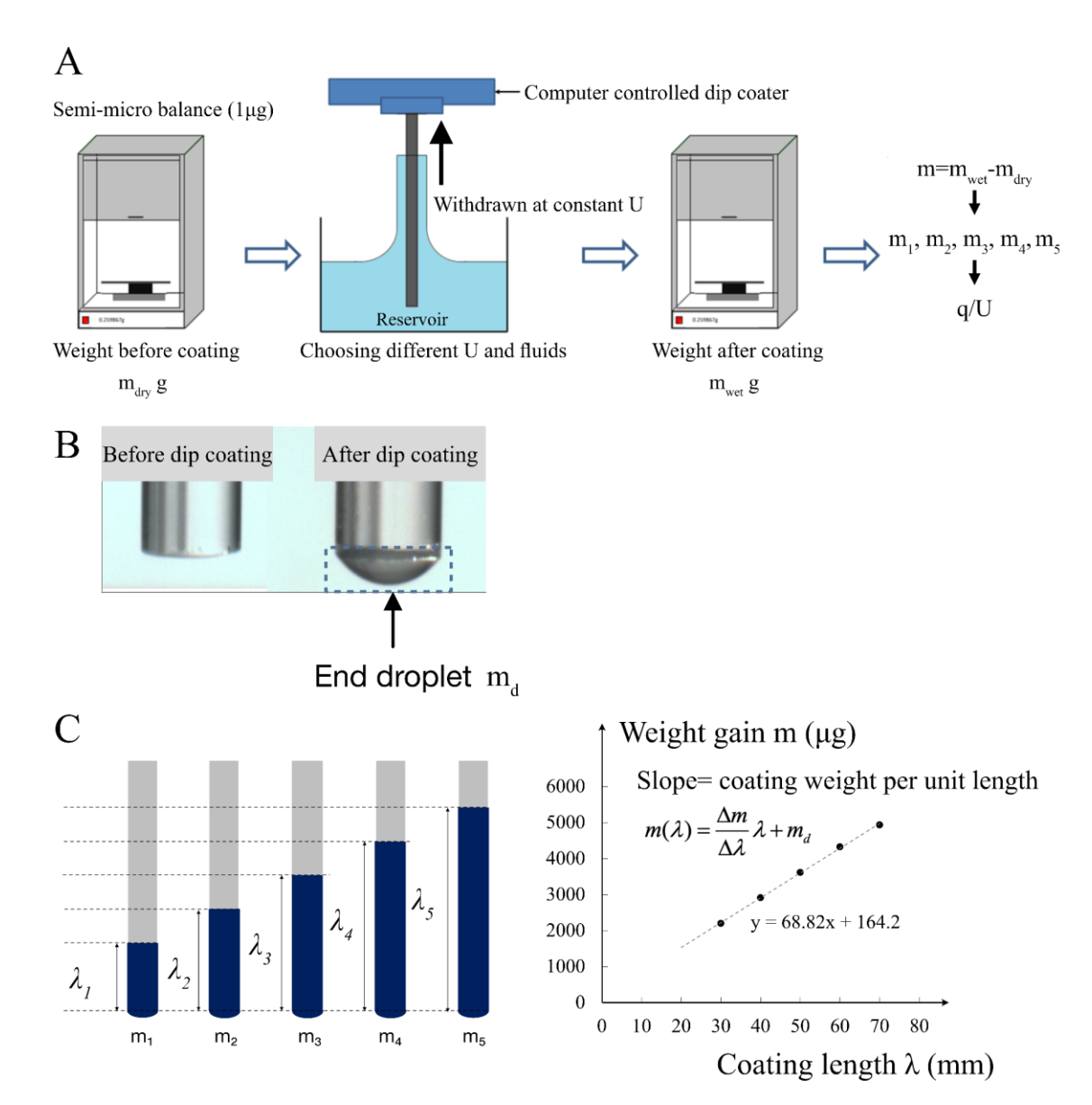


Fig. 2. (A) The schematic diagram explaining the flux thickness q/U measurements by a balance during dip coating. The mass m_{dry} of the dry rod was measured prior to the coating experiment, and the mass m_{wet} of the coated road was measured after the coating experiment. The mass $m = m_{wet} - m_{dry}$ is the weight gain at the given depth of immersion λ . (B) Illustration of an end droplet formed after dip coating. The picture on the left is taken before the coating experiment, and the picture with a drop is taken after the coating experiment. (C) To eliminate the influence of the end droplet, a series of experiments were run with different depths of immersion of the rod. The

incremental change of mass $m_{-} = m_{wet} - m_{dry}$ was calculated for each rod and plotted as a function of the depth of immersion λ_i , $1 \le i \le 5$.

3. Results and discussion

3.1. The lubrication flow model

Following the traditional scheme of the lubrication theory, we restrict ourselves to the regimes of coating at small Reynolds numbers, $Re = \rho_l U h_{\infty} / \eta \ll 1$, where h_{∞} is the film thickness; U is the withdrawal velocity; η is the viscosity of the fluid and ρ_l is its density. In our experiments, the smallest Reynolds number was 1.8×10^{-5} at R = 0.165mm, U = 20mm/min with Slygard 184; and the largest value was Re = 0.0058 at R = 0.235mm, U = 500 mm/min with hexadecane. Using the small slope approximation, one infers that the pressure p(z) is uniform across the film of thickness h(z), and pressure and the film thickness vary along the cylinder axis z. Assuming that the film is much thinner than the cylinder radius, h << R, the no-slip boundary condition at the cylinder surface moving with velocity U upwards and no shear stress condition at the air/liquid interface, r = R + h, one writes the Stokes problem in cylindrical coordinates for the z-component of velocity v as

$$-\left(\frac{dp}{dz}\right) - \rho_l g + \eta \frac{d^2 \upsilon}{dr^2} + \frac{\eta}{r} \frac{d\upsilon}{dr} = 0, \ \upsilon(R) = U, \quad \frac{d\upsilon}{dr}|_{R+h} = 0. \tag{4}$$

For thin films, h << R, the pressure gradient dp/dz is independent of the radial coordinate, and the term $(\eta/r)(dv/dr)$ is much smaller than the other three. We neglect this term and integrate (4) to infer that the velocity profile is the Poiseuillean parabolic profile [30, 46, 53]:

$$\upsilon = U + \frac{1}{\eta} \left(\frac{dp}{dz} + \rho_l g \right) (r - R) \left((r - R)/2 - h \right). \tag{5}$$

Due to definition, the flow discharge through the thin film of thickness h(z) is

$$Q = 2\pi R \int_{R}^{R+h} v dr.$$
 (6)

Substituting Eq. (5) in Eq. (6) and integrating the result, one obtains [30, 46, 53]

$$Q = 2\pi RhU - 2\pi Rh \left(\frac{h^2}{3\eta} \frac{dp}{dz}\right) - 2\pi R \frac{\rho_l g h^3}{3\eta}.$$
 (7)

Eq. (7) shows that the total flux Q(z) in the annular film at an arbitrary point z along the cylinder is due to advection, $2\pi RhU$, when the film of thickness h(z) is moving

together with the cylinder, and due to the relative motion with respect to the cylinder movement due to the pressure gradient and gravitational drainage.

When the flow is in its steady state, the flux Q should not depend on position z.

Therefore, calculating the flux at the zone of constant thickness where the film thickness is h_{∞} , and dp/dz = 0, we have from Eq. (7):

$$Q = 2\pi R \left(h_{\infty} U - \frac{\rho_l g h_{\infty}^3}{3\eta} \right) = const.$$
 (8)

We introduce the flux per unit length $q = Q/(2\pi R)$ of the cylinder circumference. Then Eq.(8) is rewritten as the ratio

$$\frac{q}{U} = h_{\infty} - \frac{\rho_l g h_{\infty}^3}{3nU}.$$
 (9)

- We call this ratio q/U the flux-based thickness, it has units of length and is directly measurable in experiments [31, 49]. When the gravitational drainage described by the term $-\rho_l g h_\infty^3/3\eta U$ in Eq. (9) is negligible, this ratio gives the coating thickness $h_\infty \approx q/U$. In the general case, $h_\infty \neq q/U$ and the measurements of the flux have to be interpreted with special care.
- Eq. (9) suggests natural constraints on the applicability of expansions (1) and (2).
 Plugging these expansions in Eq. (9) and assuming that the flux thickness is positive, one obtains that

251
$$Ca < 37.9, \quad Ca < 4.66\beta^{-3}$$
 (10)

for plates and fibers, respectively, where $\beta = R^2 \rho_l g / \sigma$ is the Bond number.

253254

255

At small capillary and Reynolds numbers, Ca, Re <<1, the distribution of pressure p in the thin film (with respect to the pressure in the surrounding air) is quasi-stationary and follows the Laplace equation of capillarity

$$p = \sigma \left(\frac{1}{R_g} + \frac{1}{R_r}\right), \quad \frac{1}{R_g} = -\frac{d\varphi}{ds}, \quad \frac{1}{R_r} = \frac{\sin\varphi}{R + h}, \tag{11}$$

where R_g and R_r are the two principal radii of curvature of the air/liquid interface, s is the arclength along the generator curve, and φ is the inclination angle introduced in Fig. 1. Assuming that s(z) increases while h(z) decreases with z, we write

$$\frac{dz}{ds} = \sin \varphi, \quad \frac{dh}{ds} = -\cos \varphi. \tag{12}$$

261 Solving Eq. (11) for $d\varphi/ds$, we have

$$\frac{d\varphi}{ds} = -\frac{p}{\sigma} + \frac{\sin\varphi}{R+h}.$$
 (13)

- Substituting Eq. (8) in Eq. (7), and resolving the pressure gradient as dp/dz =
- 264 (dp/ds)(ds/dz) and using Eq. (12) to replace ds/dz in this last equation as dp/dz =
- $(dp/ds)/\sin\varphi$, we obtain the following differential equation for the pressure gradient
- along the meridians

$$\frac{dp}{ds} = \left(3\eta U \frac{h - h_{\infty}}{h^3} - \rho_l g \left(1 - \frac{h_{\infty}^3}{h^3}\right)\right) \sin \varphi. \tag{14}$$

- 268 The system of Eqs. (12)–(14) describes the profile of the air-liquid interface, and the
- boundary conditions have to be introduced to integrate this system.

270

3.2. Dimensionless form of the governing equations and boundary conditions

- 272 Introducing the dimensionless height Z, arclength S, pressure in the film P, and local film
- 273 thickness H as

$$Z = z / R, \quad S = s / R, \quad P = p \frac{R}{\sigma}, \quad H = h / R, \quad H_{\infty} = h_{\infty} / R$$

and the capillary number, Ca, the Bond number, β , as

$$Ca = \frac{\eta U}{\sigma}, \beta = \frac{\rho_l g R^2}{\sigma},$$

277 the system of Eqs. (12)–(14) is rewritten as

$$\frac{dZ}{dS} = \sin \varphi, \tag{15}$$

$$\frac{dH}{dS} = -\cos\varphi, \quad \frac{d\varphi}{dS} = -P + \frac{\sin\varphi}{1+H},\tag{16}$$

$$\frac{dP}{dS} = \left(3\operatorname{Ca}\frac{H - H_{\infty}}{H^{3}} - \beta\left(1 - \frac{H_{\infty}^{3}}{H^{3}}\right)\right)\sin\varphi. \tag{17}$$

- The film on the rod must be matched with the static meniscus far away from the
- 282 rod where the free surface is horizontal, and the pressure in the liquid is equal to the
- atmospheric pressure. Thus, the boundary conditions are set as

284
$$S \to -\infty: P \to 0, \quad H \to \infty, \quad \varphi \to 0.$$
 (18)

285 At the positive infinity, the film is assumed uniform: 286 $S \to +\infty$: $d\varphi / dS \to 0$, $dP / dS \to 0$. Substituting these conditions in Eq. (16) and 287 Eq. (17), we obtain the following boundary conditions

288
$$S \to +\infty: \quad H = H_{\infty}, \quad P = \frac{1}{1 + H_{\infty}}, \quad \varphi = \frac{\pi}{2}. \tag{19}$$

The non-linear problem Eqs. (15)–(19) has to be solved within the infinite domain $-\infty < S < +\infty$. This non-linear problem is autonomous, i.e., the right-hand sides of all equations do not explicitly depend on S. Only the initial state, H, P, and φ , given by Eq. (18) or Eq. (19) specifies the overall solution to the problem. The solution does not depend on the choice of the initial value of the independent argument S. Thus, if functions S(S), are also the solutions for any constant S(S) to the same problem (15)–(19). This translation invariance offers a degree of freedom in choosing the reference point S(S)0 requiring a special care in formulating the boundary conditions and in the development of the numerical method to solve this problem.

One observes that the right-hand sides of Eqs. (16)–(17) for H, φ , and P do not depend on Z. Thus, they can be integrated first.

3.3. Asymptotic behavior of meniscus profile as it approaches uniform film

Formulating the coating problem, we assume that far away from the horizontal liquid-air interface, as $S \to +\infty$ and $Z \to +\infty$, the film turns into a straight $(\varphi \to \pi/2)$ cylindrical shell of thickness $H = H_{\infty}$. For any S_0 and H_{∞} , the initial value problem Eqs. (15)–(17) with initial conditions Eq. (19) must have a unique solution. For numerical integration of Eqs. (15)–(17), one has to develop an asymptotic expansion of the system at any fixed $S = S_0 >> 1$, $Z = Z_0 >> 1$.

Consider the film profile as $S \to +\infty$, $Z \to +\infty$ where the film thickness is assumed slightly deviating from its limiting thickness. Thus, we assume that $H(S) = H_{\infty} + \varepsilon(S)$ where the perturbation is small: $0 < \varepsilon(S)/H_{\infty} \ll 1$. This function $\varepsilon(S)$ is unknown yet, and we should also assume that the angle φ deviates from $\pi/2$ as $\varphi(S) = \pi/2 - \alpha(S)$, where $0 < \alpha(S) \ll 1$. Then the pressure also changes as $P = 1/(1 + H_{\infty}) - \delta(S)$, where $0 < \delta(S) \ll 1$. To find functions $\varepsilon(S)$, $\alpha(S)$ and $\delta(S)$, we substitute these representations in Eqs. (15)–(17) and Taylor expand the resulting equations with respect to $\varepsilon(S)$, $\alpha(S)$ and $\delta(S)$, to obtain in the leading order approximation as

317
$$\frac{d\varepsilon}{dS} = -\alpha, \quad -\frac{d\alpha}{dS} = \delta, \quad \frac{d\delta}{dS} = -3\left(\frac{\text{Ca}}{H_{\infty}^3} - \frac{\beta}{H_{\infty}}\right)\varepsilon. \tag{20}$$

Calculating the derivatives of the first and second equations of Eqs. (20) as

319
$$d^{3}\varepsilon / dS^{3} = -d^{2}\alpha / dS^{2}, \quad -d^{2}\alpha / dS^{2} = d\delta / dS$$

we will have from the third equation of Eqs. (20):

321
$$\frac{d^3\varepsilon}{dS^3} = -\gamma^3\varepsilon, \quad \gamma^3 = \frac{3\beta}{H_\infty} \left(\frac{\text{Ca}}{\beta H_\infty^2} - 1\right). \tag{21}$$

- 322 Assume that the following physical conditions hold true (see Supplementary material
- with the supporting experimental data)

$$\gamma > 0 \implies \text{Ca} > \beta H_{\infty}^2. \tag{22}$$

- When γ takes on a real positive value, we can integrate Eq. (21) with the condition
- 326 $\varepsilon \to 0$ at $S \to +\infty$ to find

$$H = H_{\infty} + C \exp\left(-\gamma (S - S_0)\right). \tag{23}$$

- The other flow scenarios with negative γ^3 are not considered here. The constant $C = \varepsilon(S_0)$
- 329 completely specifies the solution at an arbitrarily chosen point $S = S_0$ and determines the
- accuracy of the numerical solution of the given non-linear initial value problem.
- 331 Substituting Eq. (23) in Eqs. (20), one obtains the required asymptotic expansions
- 332 for φ and P as

333
$$\varphi = \frac{\pi}{2} - \gamma C \exp(-\gamma (S - S_0)), \tag{24}$$

334
$$P = \frac{1}{1 + H_{\infty}} - \gamma^2 C \exp(-\gamma (S - S_0)). \tag{25}$$

- Thus, Eqs. (23)–(25) specify the film behavior at the height far away from the horizontal
- 336 liquid-air interface.
- 3.4. Asymptotic behavior of meniscus profile as it approaches horizontal liquid-air
- 338 interface
- The uniform film thickness is a function of Ca and β , i.e., $H_{\infty} = f(Ca, \beta)$, and thus,
- cannot be fixed arbitrarily. For a given (Ca, β) -pair, it must be determined from the
- 341 condition that the film ultimately matches the flat air/liquid interface as $S \rightarrow -\infty$. Thus

- 342 considering H_{∞} as an unknown parameter, we apply a shooting method to solve Eq. (15)–
- 343 (17) with the initial conditions Eq. (23)–(25) at $Z_0 = 0$, $S_0 = 0$ as discussed below.
- 344 To implement the shooting algorithm, we need to study the asymptotic behavior of the
- static meniscus as it approaches the horizontal liquid/air interface. This asymptotic solution
- will then be used to select the matching condition for the shooting method.
- Following Huh and Scriven [54], the leading order asymptotic behavior of the meridian
- profile H(S) as it approaches the static meniscus is obtained by analyzing the system Eqs.
- 349 (15)–(17) as $S \to -\infty$ where $\varphi \to 0$, $H \to +\infty$. We use the asymptotic formulas
- 350 $\sin \varphi \cong \varphi$, $\cos \varphi \cong 1, \varphi \to 0, 1/(H+1)\sim 1/H, H \to +\infty$ and rewrite the system Eqs.
- 351 (15)–(17) in the form

$$\frac{dZ}{dS} = 0, \quad \frac{dH}{dS} = -1, \tag{26}$$

$$\frac{d\varphi}{dS} = -\frac{d\varphi}{dH} = -P + \frac{\varphi}{H}, \qquad (27)$$

$$\frac{dP}{dH} = \beta \varphi. \tag{28}$$

Differentiating Eq. (27) with respect to H and substituting dP/dr from Eq. (28), we have

$$\frac{d}{dH}\left(\frac{d\varphi}{dH} + \frac{\varphi}{H}\right) = \beta\varphi. \tag{29}$$

- Eq. (29) is reduced to the modified Bessel equation by introducing $x = H\beta^{1/2}$ and
- 358 multiplying Eq. (29) by x^2 :

359
$$x^2 \frac{d^2 \varphi}{dr^2} + x \frac{d \varphi}{dr} - \left(x^2 + 1\right) \varphi = 0, \quad \varphi \to 0, \quad x \to +\infty. \tag{30}$$

- 360 The modified Bessel function of the second kind satisfies Eq. (30) with the required
- 361 condition $\varphi \to 0$ at $x \to +\infty$:

$$\varphi(H) = C_2 K_1 \left((1+H)\beta^{1/2} \right), \quad H \to +\infty, \tag{31}$$

- where C_2 is an integration constant. Substituting Eq. (31) in Eq. (27) and solving it for P,
- 364 we find

365
$$P(H) = C_2 \left(\frac{1}{1+H} K_1 \left((1+H)\beta^{1/2} \right) - \dots \frac{1}{2} \left(K_0 \left((1+H)\beta^{1/2} \right) + K_2 \left((1+H)\beta^{1/2} \right) \right) \right), H \to \infty. \quad (32)$$

366 The ratio $P(H)/\varphi(H)$ does not depend on constant C_2 :

367
$$B(H) = \frac{P(H)}{\varphi(H)} = \frac{1}{1+H} - \beta^{1/2} \frac{K_0 \left((1+H)\beta^{1/2} \right) + K_2 \left((1+H)\beta^{1/2} \right)}{2K_1 \left((1+H)\beta^{1/2} \right)}, \ H \to \infty.$$
 (33)

- 368 This condition is used in our shooting method to correct the guess value of the film
- thickness H_{∞} . 369
- 370 3.5. The idea of the shooting method for numerical integration of Eqs. (15)–(19)
- 371 For any pair of dimensionless parameters Ca and β satisfying inequality Eq. (22), the
- problem (15)–(17) with the initial conditions (23)–(25) at $Z_0 = 0$, $S_0 = 0$ has a set of 372
- solutions in the entire infinite interval $-\infty < S < +\infty$. Each solution corresponds to a 373
- particular positive value of the constant film thickness at infinity, H_{∞} . However, to solve 374
- 375 the boundary value problem including conditions (29)–(33), one has to select a unique
- 376 value $H_{\infty}(Ca, \beta)$ among the obtained solutions of the initial value problem that corresponds
- 377 to a particular overall film configuration. The latter is prescribed by the boundary
- 378 conditions Eq. (18) The developed shooting method numerically selects this unique
- 379 solution.
- 380 The algorithm is as follows. For the given Bond number β and capillary number Ca, we
- use Eqs. (1) and (2) to find γ . This will be our first guess. Using this γ , one solves Eq. (21) 381
- to obtain H_{∞} and using Eqs. (23)–(25), one obtains the initial conditions for H, P, and φ . 382
- To numerically integrate the obtained system (15)–(19), we take advantage of translational 383
- invariance of the problem (15)–(19) and introduce an auxiliary system of coordinates with 384
- $Z_0 = 0$, $S_0 = 0$. 385
- At the given guess values of H_{∞} and γ numerical integration of Eqs. (15)–(17) is proceeded 386
- along S toward the meniscus at negative infinity by putting $C = 10^{-8} H_{\infty}$. With this choice 387
- of constant C, we guarantee a sufficiently accurate numerical solution of the problem, Eqs. 388
- (15)–(19). The goal is to distinguish such a unique film thickness $H_{\infty}(Ca, \beta)$ that the film 389
- profile renders flat at $S \to -\infty$, i.e., the inclination angle φ and the pressure P become 390
- vanishingly small. The interface profile is considered "numerically flat" when the angle φ 391
- reaches $\varphi_* = 10^{-8}$. At this point $\varphi = \varphi_*$ and the corresponding $S = S_*$, we obtain a set of
- 392
- numeric values $H = H_*$, $P = P_*$, and $Z = Z_*$. The film thickness H_{∞} is considered the 393
- final solution when the ratio $B_* = P_*/\varphi_*$ and the value $B(H^*)$, calculated from Eq. (33) 394
- 395 become equal to one another.

We thus, reduce the problem of finding the film thickness $H_{\infty} = H_{\infty}(Ca, \beta)$ to a problem of 396 minimization of the following function 397

398
$$J(H_{\infty}) = (B(H_*) - B_*)^2 \to \min_{H_{\infty}},$$
 (34)

with respect to H_{∞} at the fixed Ca and β . 399

400 This minimization problem, Eq. (34), is solved with the use of the built-in MatLab function fminsearch. Iteratively changing H_{∞} , the MatLab implementation of Eq. (34) calls for numerical integration of Eqs. (15)–(19) at a new value $\gamma(H_{\infty})$, and so the iteration process 402 continues until the condition, $B(H_*) = B_*$ is met. However, at every H_∞ at the fixed pair 403 Ca and β , a vanishingly small value $\varphi_* = 10^{-8}$ was not observed in the solution to the 404 problem (15)–(19). How we deal with this situation is discussed in Supplementary 405 406 Information. Once the thickness H_{∞} has been found, the shooting algorithm is considered completed 407 and the solution $\{H(S,Ca,\beta), P(S,Ca,\beta), \varphi(S,Ca,\beta), Z(S,Ca,\beta)\}$ with the dependence 408

 H_{∞} (Ca, β) is reported. To bring all obtained profiles to the same horizontal liquid/air interface, we subtract the obtained constant $Z_*(H_\infty)$ from each Z and plot H = H(Z - Z_*, H_{∞}). This way, the starting height of integration is shifted to $Z = Z_*$ at $S = S_0$.

411

412

413

409

410

401

3.6. Comparison with LLD theory and analytical approximation of the numerical solutions for the film thickness

414 415

In order to compare our results with the LLD theory for fibers and plates, in Fig. 3 we plot 416 by dashed lines the pre-factors in Eq. (1) and Eq. (2), and by solid curves – the dependence 417 of $h_{\infty}l^{-1}Ca^{-\frac{2}{3}}$ on R/l calculated using the discussed algorithm. When the rod radius is 418 much smaller than the capillary length, R/l < 0.1, our calculations match the predictions 419 of the LLD theory for fibers, Eq. (2). At very small rod radii, the film thickness depends 420 421 on the rod radius linearly as predicted by Eq. (35). Increasing the rod radius, one expects 422 to form a thicker coating. However, at R/l > 0.1 we observe a divergence from the fiber LLD theory and transition to the plate theory, Eq. (1). In the transition region, 0.1 < R/l < 10423 424 10, the calculated film thickness is smaller than the film thickness predicted by the LLD 425 theory for fibers and for plates. The transition from the fiber-like to plate-like behavior 426 occurs as the rod radius approaches the capillary length, $R \sim l$. In this range of the rod radii, the weight of the meniscus becomes important, and hence the film thickness changes 427 428 significantly.

The behavior of capillary number is more complex. The scaling $h_{\infty} \propto C a^{\frac{2}{3}}$ falls short as 429 the capillary number increases above $Ca > 10^{-2}$, the red curves in Fig. 3. The proposed 430

model, Eqs. (15)–(17), predicts that the coating thickness on fibers should be greater than the LLD thickness, Eq. (2).

Thus, the modified LLD model in hands captures new phenomena and it is interesting to compare it with the results of coating experiments.

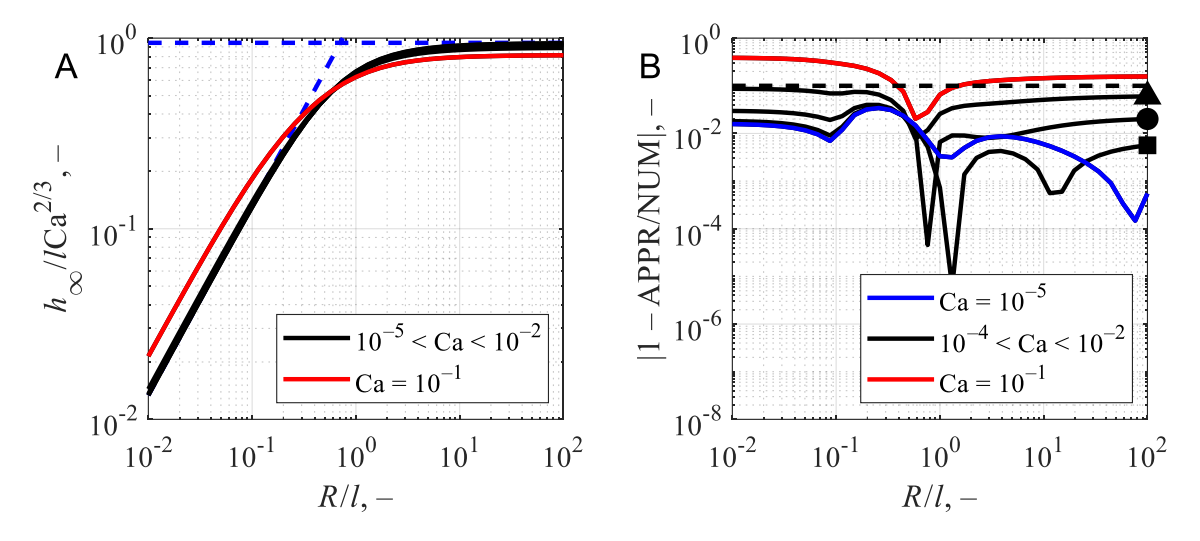


Fig. 3. (A) The comparison of the LLD theory pre-factors A_{plate} , $A_{fiber}R/l$ (the dashed lines) defined by Eqs. (1)–(2) and the results of numerical analysis (the solid curves) of the model Eqs. (15)–(17) and (23)–(25) for $10^{-2} \le R/l \le 10^2$. For small capillary numbers, $Ca < 10^{-2}$, all numeric results fall on the same curve suggesting a universal scaling with Ca number. (B) The relative difference (the solid curves) between the approximate Eqs.(36)–(39) (APPR) and the calculated h_{∞} -values (NUM) from (A) at different Ca numbers. Triangle – $Ca = 10^{-2}$, circle – $Ca = 10^{-3}$, square – $Ca = 10^{-4}$. The dashed line is the constant value 10^{-1} , showing the accuracy of the approximate Eqs.(36)–(39).

To approximate the dependence of h_{∞} / (lCa^{2/3}) on a single dimensionless parameter β , we use the scaled Langevin and Brillouin functions as

446
$$\frac{h_{\infty}}{l \text{Ca}^{2/3}} = \begin{cases} B_J(x_B), & \beta < 10^{-2}; \\ L(x_L), & \beta > 10^{-2}; \end{cases}$$
 (36)

447 where

$$L(x_L) = A_{plate} \left(\coth x_L - \frac{1}{x_L} \right)$$
 (37)

449
$$B_{J}(x_{B}) = 0.51 \left(\frac{2J+1}{2J} \coth \left(\frac{2J+1}{2J} x_{B} \right) - \frac{1}{2J} \coth \left(\frac{x_{B}}{2J} \right) \right), \quad J = 0.14 \quad (38)$$

450 and

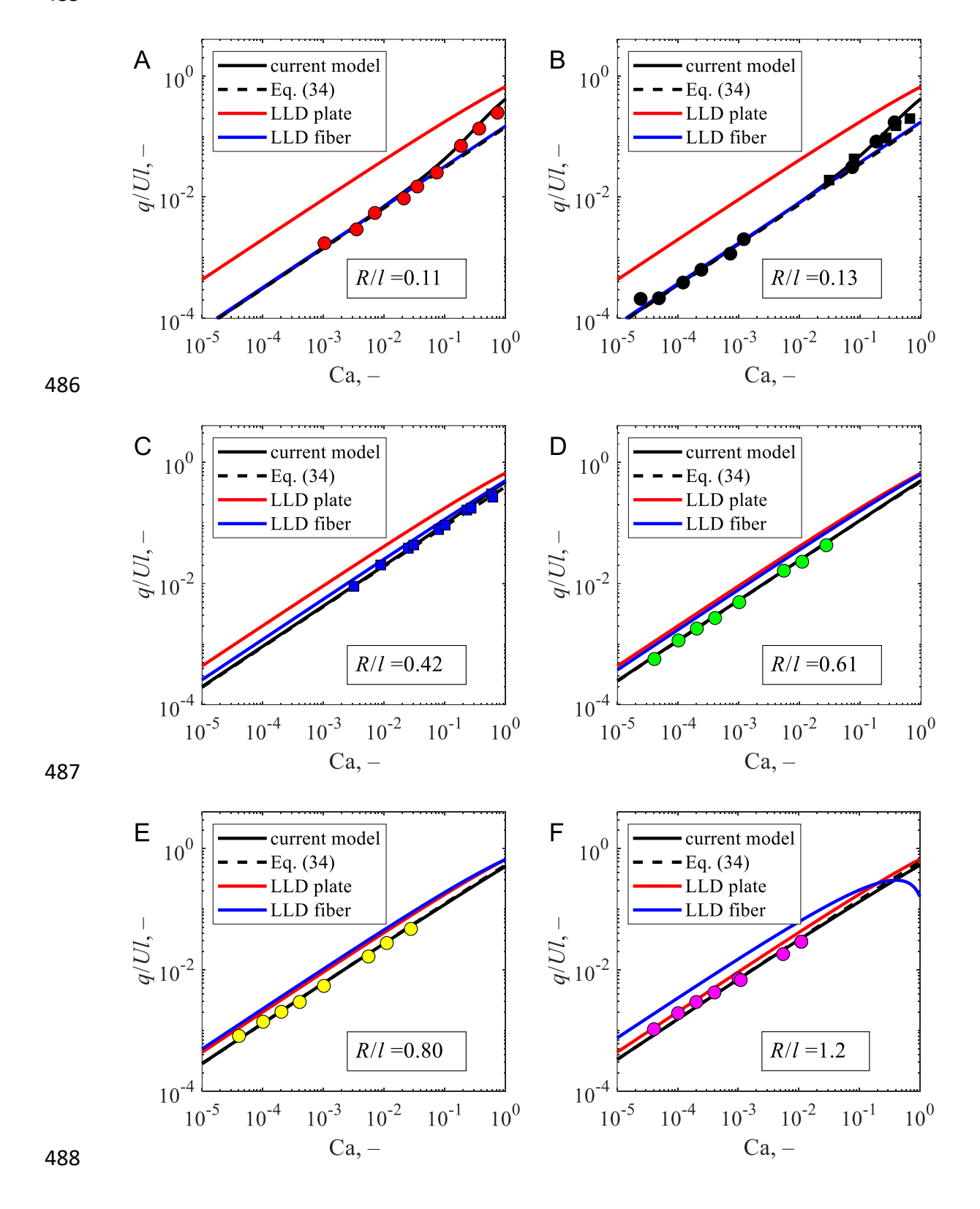
465

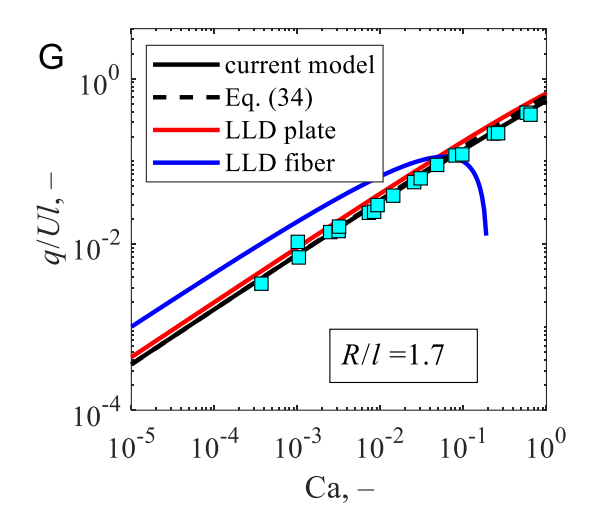
451
$$x_L(\beta) = \frac{4.5}{A_{fiber}} \beta^{1/2.2}, \quad x_B(\beta) = 1.1 \left(\frac{\beta}{A_{fiber}}\right)^{1/2}.$$
 (39)

- The accuracy of this approximation is shown in Fig. 3B. The smaller the capillary number,
- 453 the better this approximation is. Below is an example of how to use Eq. (36)–(39) to predict
- 454 the coating thickness h_{∞} .
- 455 Assume the following physical parameters for the liquid/rod pair relevant for Conostan
- 456 S60: $\rho_l = 869 \text{ kg/m}^3$, $\sigma = 30.9 \text{ mN} / \text{m}$, R = 1.15 mm, $\eta = 102 \text{ mPa·s}$, U = 0.00167 m / s.
- 457 Accordingly, Ca = 5.50×10^{-3} , and $\beta = 0.364 > 10^{-2}$. As shown in Eq (36), calculating the
- 458 Bond number β, we observe that the Langevin function should be used for this Bond
- number, $h_{\infty}/(lCa^{2/3}) = L(x_L)$. Substituting the calculated Bond number in the first
- equality of Eq. (39), we obtain $x_L = 2.13$, and calculating the Langevin function using Eq.
- 461 (37), we have L(2.13) = 0.528. Using Eq. (36), with $L(x_L) = 0.528$, we estimate the film
- 462 thickness for these physical conditions as $h\infty = 31.3 \mu m$. The experimental thickness is 31.0
- 463 µm (as shown in Table S1). Thus, the difference of the approximate thickness and the
- experimental value is measured in 1%.

3.7. Comparison with experiments

- In Fig. 4 we plot the flux-based film thickness as a function of capillary number Ca for
- different rods and compare these data with different theories and experiments.
- Within the whole range of investigated capillary numbers, $10^{-5} < Ca < 10^{-1}$, and
- 469 capillary lengths, 0.11 < R/l < 1.7, the experimental data are crowded below the LLD theory
- 470 predictions for the plates, the red curves. The thin rods, R/l = 0.11, 0.13, can be treated as
- 471 the LLD fibers. For small capillary numbers, $Ca < 10^{-1}$, and $R/l \le 0.13$, the LLD theory for
- fibers completely explains the experiments. For the rods R/l = 0.13, the White-Tallmadge
- data[31] and our experiments cover a broad range of capillary numbers $10^{-5} < Ca < 10^{0}$.
- All these data can be explained by the proposed model, suggesting that the flow under the
- 475 meniscus does not affect the coating thickness significantly. Even at the range of capillary
- numbers $Ca > 10^{-2}$ where the trend changes significantly from that of the classical LLD
- 477 theory, the proposed theory predicts the correct flux-based thickness q/U.
- As the rod radius increases above R/l > 0.13, we start to observe deviations from the LLD
- 479 theory for fibers. The flux-based thickness predicted by the LLD theory is always greater
- than that observed in experiments and predicted by the proposed model.
- When the rod radius approaches the capillary length, $R \sim l$, the LLD predictions of the
- coating thickness for plates become closer to the experimental data, yet overestimate them.
- We expect that the LLD theory for plates should satisfactorily explain the experimental
- data when the rod radius increases above R > 1.7l.





491 492

493

494

495

496

497

498 499

500

501

502

503

504

505

506

507

508

509 510

511

512513

Fig. 4. Comparison of different theories with experimental data of White and Tallmadge[31] (squares) and of this work (circles) measured at various R/l ratios (A) 0.11, (B) 0.13, (D) 0.42, (E) 0.61, (F) 0.80, (G) 1.2, (H) 1.7. All points satisfy Eq. (20) based on the calculated value H_{∞} . The flux-based thickness q/U calculated for the LLD fiber approximation based on Eqs. (2) and (9) turns negative at large β and Ca as indicated by the blue curve rapidly bending down in (F) and (G). The second inequality (for fibers) in Eq. (10) is not satisfied for particular (Ca, β) combinations. In every calculation the obtained H_{∞} -value satisfies the constraint (22).

Fig. 5 (A) summarizes the comparison of experimental data versus predictions of the modified LLD theory. This graph confirms that the proposed model Eqs. (15)–(17), (23)– (25) does predict the coating thickness on cylinders with the dimensionless thicknesses of R/l = 1.7, 1.2, 0.80, 0.61, 0.42, 0.13, 0.11, for a broad range of capillary numbers $(10^{-5} < Ca < 10^{-1})$. Fig. 5 (B) shows the relative difference between the theoretical (NUM) and experimental (EXP) thickness as a function of the Bond number. The typical difference does not exceed 30%, and the majority of points is crowded below 20%, while for individual data points may reach up to 33%. The only outlier is a single point from the White-Tallmadge experiment at R/l = 0.13. In our experiments at small capillary numbers when the coating thickness was very small, the evaluation of its weight was less accurate compared to that obtained at the larger capillary numbers. The White-Tallmadge data points for R/l = 1.7 at low capillary $Ca \approx 10^{-3}$ numbers probably suffer the same problem. To verify the White-Tallmadge data on the R/l = 0.13 rods at larger capillary numbers, $Ca > 10^{-2}$, we repeated these experiments to show that the proposed theory does explain the experimental data for Ca < 0.366 but for greater capillary numbers the deviation from the theoretical trend becomes significant. Therefore, the behavior of meniscus and the change of its shape with capillary number was studied. The results are demonstrated in Fig. 6.

515

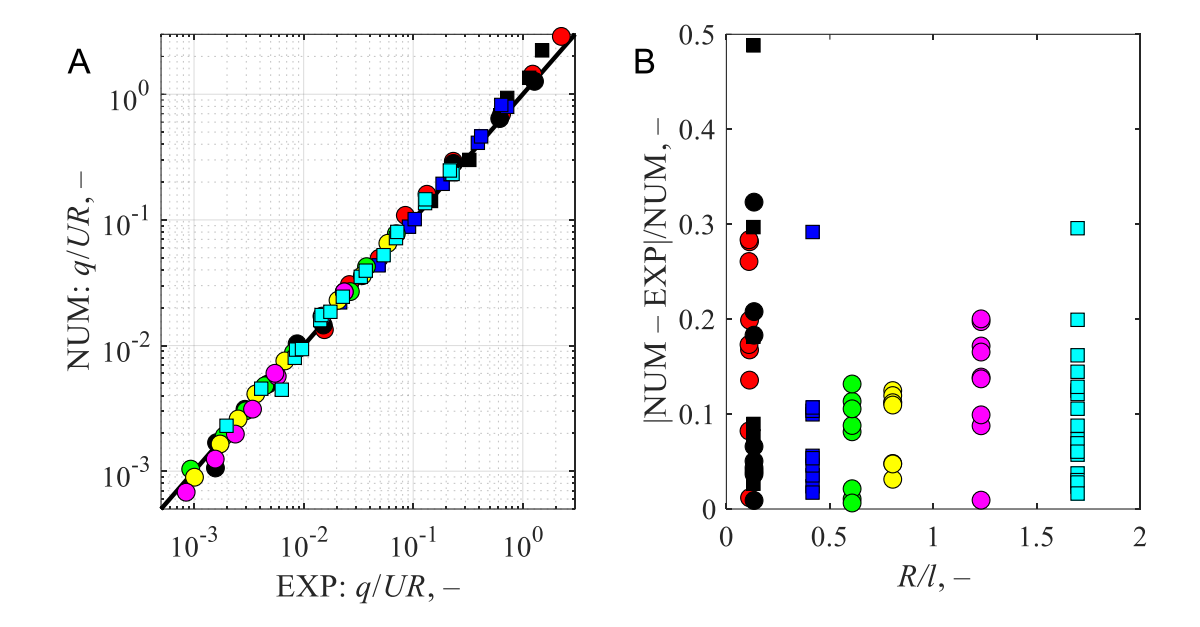


Fig. 5. (A) The collected results of experiments and theoretical predictions of the coating thickness at different conditions. The circles correspond to this work and the squares are taken from the White and Tallmadge work. (B) The relative difference between the numerical flux thickness (NUM) and the experimental one (EXP).

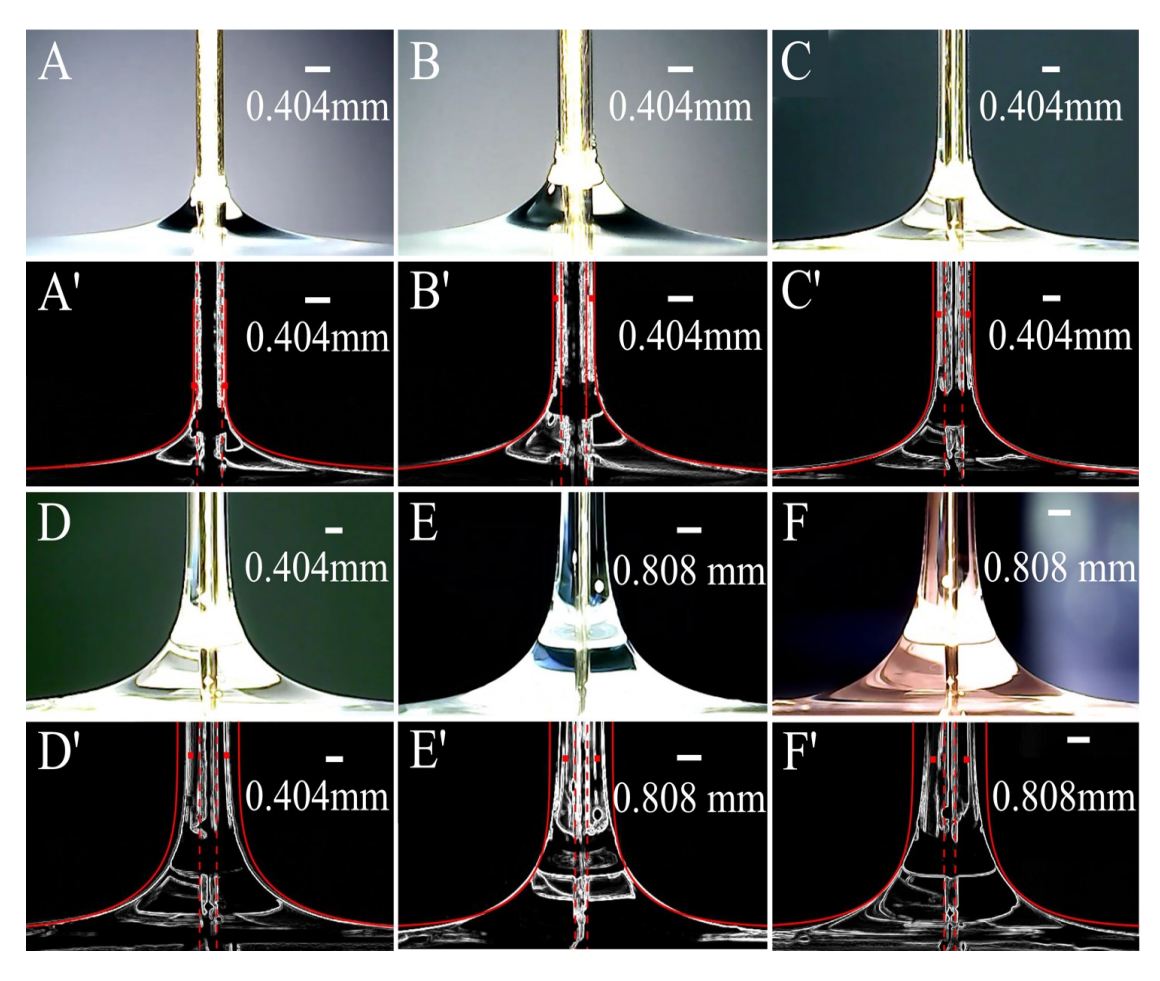


Fig. 6. (A)-(F) Images of dynamic menisci for a brass wire (R=0.202mm, R/l=0.13) drawn at different U out of a bath of Sylgard 184. (A')-(F') The binarized images of dynamic menisci and the menisci contours predicted by the theory, Eqs. (15)–(19). The red squares show the coating film thickness h_{∞} on the fiber predicted by Eq. (2). (A)(A') U=20mm/min, Ca=0.0732, (B)(B') U=50mm/min, Ca=0.183, (C)(C') U=100mm/min, Ca=0.366, (D)(D') U=200mm/min, Ca=0.732, (E)(E') U=350mm/min, Ca=1.28, (F)(F') U=500mm/min, Ca=1.83.

When the capillary number is small, Ca < 0.366, the theoretical profiles of menisci closely follow the experimentally observed profiles. Eq. (2) for fibers also predicts the film thickness h_{∞} with acceptable accuracy. Thus, the lubrication theory captures the main features of film flow in this regime of rod coating. This shows the model does a good job capturing the fine features of menisci, which cannot be described by ignoring the nonlinear meniscus curvature at the transition region. Thus, the two-way experimental analysis using the weight method and imaging of meniscus profiles confirms the proposed idea of the importance of both principal curvatures of meniscus in film shaping in the transition region and control of the coating thickness. However, as one increases the capillary number above Ca > 0.366, the theoretical profiles of menisci move away from the experimentally observed ones, overestimating the thickness h_{∞} . White and Tallmadge suspected that the

size of liquid reservoir may influence the meniscus shape and hence the coating thickness [31]. To evaluate this effect, two tubes of radii (R_t =13.0 mm, 23.5 mm) were examined. These tubes were filled with S60 to the same height. The rods of radii R=0.500 mm, 2.35 mm were coated from these tubes at velocity U=500 mm/min, and U=200 mm/min.

Table 3 summarizes the results of these experiments. Comparing Experiment No.1 against Experiment No. 2, one observes that the flux-based thickness $\frac{q}{u}$ remains nearly unchanged; a pair of Experiment No. 3 and No. 4 confirms this observation. Thus, when the ratio of the rod radius to the tube radius is small, the meniscus shape is not affected by the tube size and hence the divergence of the observed experimental thickness from the LLD theory cannot be explained by the effect of the flow confinement.

Table 3 Dimensionless flux-based thickness in different containers

Experiment No.	1	2	3	4
Capillary number	0.028	0.028	0.011	0.011
Rod radius (mm)	0.500	0.500	2.35	2.35
Reservoir radius (mm)	13.0	23.5	13.0	23.5
R_t/R	26	47	5.5	10
R/l	0.26	0.26	1.2	1.2
Flux-based thickness(μm)	49.9	50.1	55.0	55.1

Summary of key findings. With the progress of fiber technology and new coating materials,

Conclusion

540 541

542

543

544

545

546

547

548 549

550

551

552

553

554 555

556

557

558 559

560

561

562

563 564

565

566 567

568

569 570

571

572

the demand for understanding of controlling parameters for the dip-coating method is high [23, 44, 45]. In this paper, we study the effect of the rod radius, withdrawal velocity, surface tension, viscosity, and density of liquid finishes used in the dip coating processes of cylindrical articles. These data significantly enrich the available data set obtained earlier by White and Tallmadge [31, 49]. To explain the experimental results, we developed a new mathematical model; the theoretical predictions of the behavior of coating films on the process parameters are given in Fig. 4 and Fig. 5. We showed that the classical LLD model falls short of describing the experimental data on rods for capillary numbers greater than Ca > 10^{-2} . While the LLD scaling $h_{\infty} \propto lCa^{\frac{2}{3}}$ on capillary number Ca < 1 appears useful, the ratio $h_{\infty}l^{-1}Ca^{-\frac{2}{3}}$ significantly deviates from the LLD predictions for rods having the radii greater than R/l > 0.1. The film thickness is always smaller than that predicted by the LLD theory. Highlights of the hypothesis, new concepts, and innovations. We hypothesized that the predictions of LLD theory can be improved by restoring the non-linear meniscus curvature in the equation for the flow of a coating film. We used the Laplace equation of capillarity in its full non-linear form. This modification allowed us to use the shooting method to numerically solve the obtained set of non-linear differential equations with non-linear boundary conditions. All the processing parameters were collapsed into the capillary number Ca and the ratio of the rod radius to the capillary length, R/l. The model

- 573 predictions were verified by experiments. A large range of capillary numbers from 10^{-5}
- to 10^{-1} was covered to show that the proposed model does explain the experimental data
- with a good accuracy. An approximate set of analytic Eqs. (36)–(39) was derived to predict
- 576 the coating thickness h_{∞} .
- 577 Future developments and engineering and materials science applications. The developed
- 578 model and experimental protocols could be used in many applications dealing with coating
- of different rods. While the numerical analysis of the dip coating problem using Navier-
- 580 Stokes equations with the free boundary [55-58] is very attractive as it sheds new light on
- the flow phenomena, a significant benefit of the presented 1D model is in its practicality
- and simplicity. The analytical representation of the film thickness dependence on capillary
- and Bond numbers Eqs. (36)–(39) allows one to straightforwardly use it for design of the
- rod finishing protocols with the desired outcome. The paper provides a new insight on the
- 585 classical problem of dip coating of rods and significantly expands the library of
- experimental data on different rods and finishes. The problem concerns not only engineers.
- Mouth parts of many insects are fiber-like and the process of insect feeding somewhat
- resembles a process of fiber dip coating [59]. Therefore, the results of this work can be used
- 589 for analysis of insect behavior during feeding.

Acknowledgements

590

- 591 Z.Z. and F.P would like to thank the funding support from NIH P20GM121342. The
- lubrication flow model was partially developed by A.S., and he is thankful to the
- 593 government assignment for FRC Kazan Scientific Center of RAS. The development and
- verification of numerical algorithm to solve the model equations was supported by the
- 595 Ministry of Science and Higher Education of the Russian Federation under agreement
- No. 075-15-2020-931 within the framework of the development program for a world-
- 597 class Research Center "Efficient development of the global liquid hydrocarbon reserves".
- 598 K.G.K. was partially supported by National Science Foundation award IOS- 2042937 and
- the SC EPSCoR/IDeA Program under NSF Award No. OIA-1655740. The views,
- perspectives, and content do not necessarily represent the official views of the SC
- 601 EPSCoR/IDeA Program northose of the NSF.

Table of parameters

Са	Capillary number $Ca = \frac{U\eta}{\sigma}$
g	Acceleration due to gravity
h(z)	The film profile
h_{∞}	Coating thickness at the constant thickness region
l	Capillary length $\boldsymbol{l} = \sqrt{\frac{\sigma}{\rho g}}$
m _d	Mass of the end droplet
M _{dry}	Mass of the rod before dip-coating
m _{wet}	Mass of the rod after dip-coating
m (λ)	Mass gain with a coating of λ
Z	Vertical coordinate in a moving system
p	Pressure
q	Circumferential flux of coating liquid on the rod
Q	Flux of coating liquid on the rod
R	Radius of the cylinder
R_t	Radius of the reservoir
R_g, R_r	Two principal radii of curvature of the air/liquid interface
r	Coordinate in the radial direction

S	Arclength along the generator curve of air/liquid interface
υ	Vertical component of fluid velocity distribution as a function of radial coordinate r
U	Withdrawal velocity of the cylinder
Z	Coordinate in the vertical direction
$ ho_l$	Density of coating fluid
λ	Coating length
β	Bond number
σ	Surface tension of coating fluid
к	Local curvature of the air/liquid interface
η	Viscosity of coating fluid
φ	Local inclination angle of the generator curve of air/liquid interface

607

References

- [1] S.E. Kistler, P.M. Schweizer, Liquid film coating. Scientific principles and their technological implications, Chapman & Hall, Glasgow, UK, 1997, p. 783.
- [2] A. Jonsson, A. Roos, E.K. Jonson, The effect on transparency and light scattering of dip coated antireflection coatings on window glass and electrochromic foil, Sol. Energy Mater. Sol. Cells 94(6) (2010) 992-997.
- [3] D. Sui, Y. Huang, L. Huang, J. Liang, Y. Ma, Y. Chen, Flexible and transparent electrothermal film heaters based on graphene materials, Small 7(22) (2011) 3186-615 92.
- [4] E. Mohseni, E. Zalnezhad, A.R. Bushroa, Comparative investigation on the adhesion of hydroxyapatite coating on Ti-6Al-4V implant: A review paper, International Journal of Adhesion and Adhesives 48 (2014) 238-257.
- [5] D. Janas, K.K. Koziol, A review of production methods of carbon nanotube and graphene thin films for electrothermal applications, Nanoscale 6(6) (2014) 3037-45.
- [6] B. Mahltig, H. Haufe, H. Bottcher, Functionalisation of textiles by inorganic sol-gel coatings, Journal of Materials Chemistry 15(41) (2005) 4385-4398.
- [7] B. Mahltig, H. Böttcher, Modified silica sol coatings for water-repellent textiles, Journal of Sol-Gel Science and Technology 27(1) (2003) 43-52.

- [8] K.K. Chawla, Z.R. Xu, J.S. Ha, M. Schmucker, H. Schneider, Effect of BN coating on
- the strength of a mullite type fiber, Appl. Compos. Mater. 4(5) (1997) 263-272.
- 627 [9] M. Seo, Y. Akutsu, H. Kagemoto, Preparation and properties of Sb-doped
- 628 SnO2/metal substrates by sol-gel and dip coating, Ceramics International 33(4)
- 629 (2007) 625-629.
- [10] J.O. Park, A.D. Rey, M. Srinivasarao, Non-classical scaling for forced wetting of a
- nematic fluid on a polymeric fiber, Soft Matter 5(11) (2009) 2277-2280.
- 632 [11] A.D. Rey, Analysis of liquid crystalline fiber coatings, Molecular Crystals and
- 633 Liquid Crystals Science and Technology Section a-Molecular Crystals and Liquid
- 634 Crystals 333 (1999) 15-23.
- 635 [12] K.S. Wang, R.K. Bordia, L.N. Brush, A semi-empirical power-law model for the
- dip-coating of a substrate into a particle-containing, non-Newtonian, complex fluid
- 637 system, Ceramics International 45(6) (2019) 6655-6664.
- 638 [13] K. Afanasiev, A. Muench, B. Wagner, Landau-Levich problem for non-Newtonian
- 639 liquids, Physical Review E 76(3) (2007).
- [14] J. Ashmore, A.Q. Shen, H.P. Kavehpour, H.A. Stone, G.H. McKinley, Coating flows
- of non-Newtonian fluids: weakly and strongly elastic limits, Journal of Engineering
- 642 Mathematics 60(1) (2008) 17-41.
- [15] P. Daripa, G. Pasa, The thickening effect of interfacial surfactant in the drag-out
- coating problem, Journal of Statistical Mechanics-Theory and Experiment (2009).
- 645 [16] H.N. Dixit, G.M. Homsy, The elastocapillary Landau-Levich problem, Journal of
- 646 Fluid Mechanics 735 (2013) 1-28.
- 647 [17] H.N. Dixit, G.M. Homsy, The elastic Landau-Levich problem, Journal of Fluid
- 648 Mechanics 732 (2013) 5-28.
- 649 [18] Gutfinge.C, Tallmadg.Ja, Films of non-newtonian fluids adhering to flat plates,
- 650 Aiche Journal, 1965, pp. 403-&.
- 651 [19] M. Ouriemi, G.M. Homsy, Experimental study of the effect of surface-absorbed
- 652 hydrophobic particles on the Landau-Levich law, Physics of Fluids 25(8) (2013).
- 653 [20] R.P. Spiers, C.V. Subbaraman, W.L. Wilkinson, Free coating of a Newtonian liquid
- onto a vertical surface, Chemical Engineering Science 29(2) (1974) 389-396.
- 655 [21] R.L. Cerro, Moving contact lines and Langmuir-Blodgett film deposition, Journal
- of Colloid and Interface Science 257(2) (2003) 276-283.
- 657 [22] M. Ghosh, F.Q. Fan, K.J. Stebe, Spontaneous pattern formation by dip coating of
- colloidal suspensions on homogeneous surfaces, Langmuir 23(4) (2007) 2180-2183.
- 659 [23] E. Rio, F. Boulogne, Withdrawing a solid from a bath: How much liquid is coated?,
- Advances in Colloid and Interface Science 247 (2017) 100-114.
- 661 [24] M. Maleki, M. Reyssat, F. Restagno, D. Quere, C. Clanet, Landau-Levich menisci, J
- 662 Colloid Interface Sci. 2011, pp. 359-363.
- 663 [25] R.G.C. Arridge, D. Heywood, The freeze-coating of filaments, British Journal of
- 664 Applied Physics 18(4) (1967).
- [26] H. Levy, A.J. Lockyer, R.G.C. Arridge, Coating of fibers, Int. J. Heat Mass Transf.
- 666 21(4) (1978) 435-443.

- 667 [27] H. Chen, F. Tian, J. Kanka, H. Du, A scalable pathway to nanostructured sapphire
- optical fiber for evanescent-field sensing and beyond, Applied Physics Letters
- 669 106(11) (2015) 5.
- 670 [28] V.S. Shevandin, A single-mode microstructured lightguide with a large core in a
- 671 metallic coating, J. Opt. Technol. 82(2) (2015) 116-119.
- [29] D. Quere, Fluid coating on a fiber, Annual Review of Fluid Mechanics 31 (1999)
- 673 347-384.
- [30] B.V. Deryagin, Theory of the deposition of a viscous liquid on to-a fiibre or wire
- being-withdrawn from the liquid., Prikl. Mekh. Tekh. Phys. 3 (1963) 71-78.
- 676 [31] D.A. White, J.A. Tallmadge, A theory of withdrawal of cylinders from liquid baths,
- 677 Aiche J. 12(2) (1966) 333-339.
- 678 [32] K.G. Kornev, A.V. Neimark, Hydrodynamic instability of liquid films on moving
- 679 fibers, Journal of Colloid and Interface Science 215(2) (1999) 381-396.
- 680 [33] A. Ghosh, D. Bandyopadhyay, A. Sharma, Micro-patterning of coatings on a fiber
- 681 surface exploiting the contact instabilities of thin viscoelastic films, Physics of Fluids
- 682 30(11) (2018).
- [34] Y.P. Huang, T.K. Chen, L.C. Row, F.L. Chen, Effect of surface treatment and wetting
- 684 behavior on fiber surface and resulted yarn property, Colloids and Surfaces a-
- Physicochemical and Engineering Aspects 307(1-3) (2007) 108-115.
- 686 [35] S. Ravinutala, C. Polymeropoulos, Entrance meniscus in a pressurized optical
- fiber coating applicator, Exp. Therm. Fluid Sci. 26(5) (2002) 573-580.
- 688 [36] E. Ruckenstein, Scaling analysis of coating of a plate or a fiber, Journal of Colloid
- and Interface Science 246(2) (2002) 393-400.
- 690 [37] D.B. Gundel, P.J. Taylor, F.E. Wawner, Fabrication of thin oxide coatings on
- ceramic fibers by a sol-gel technique, Journal of Materials Science 29(7) (1994) 1795-
- 692 1800.
- 693 [38] E. Boakye, R.S. Hay, M.D. Petry, Continuous coating of oxide fiber tows using
- 694 liquid precursors: Monazite coatings on Nextel 720 (TM), Journal of the American
- 695 Ceramic Society 82(9) (1999) 2321-2331.
- 696 [39] M. Verdenelli, S. Parola, F. Chassagneux, J.M. Letoffe, H. Vincent, J.P. Scharff, J.
- 697 Bouix, Sol-gel preparation and thermo-mechanical properties of porous xAl(2)0(3)-
- 698 ySiO(2) coatings on SiC Hi-Nicalon fibres, Journal of the European Ceramic Society
- 699 23(8) (2003) 1207-1213.
- 700 [40] E. Shim, Coating and laminating processes and techniques for textiles, 2019.
- 701 [41] F. Kern, R. Gadow, Deposition of ceramic layers on carbon fibers by continuous
- 702 liquid phase coating, Surf. Coat. Technol. 180 (2004) 533-537.
- 703 [42] F.A. Reifler, F.A.L. Sanchez, F.J. Clemens, K. Varga, R. Hufenus, Flexible ceramic-
- 704 reinforced polyurethane composite coatings on synthetic fibres: Process of
- 705 continuous liquid film coating and its influence on the coating thickness, Composites
- 706 Science and Technology 70(8) (2010) 1207-1213.
- 707 [43] P. Yimsiri, M.R. Mackley, Spin and dip coating of light-emitting polymer solutions:
- 708 Matching experiment with modelling, Chemical Engineering Science 61(11) (2006)
- 709 3496-3505.
- 710 [44] K.J. Ruschak, Coating flows, Annual Review of Fluid Mechanics 17 (1985) 65-89.

- 711 [45] S.J. Weinstein, K.J. Ruschak, Coating flows, Annual Review of Fluid Mechanics 36
- 712 (2004) 29-53.
- 713 [46] L. Landau, B. Levich, Dragging of a liquid by a moving plate, Acta Physicochimica
- 714 URSS 17 (1942) 42-54.
- 715 [47] B.V. Derjaguin, Thickness of the liquid film adhering to a moving thread, Doklady
- 716 Akademii Nauk SSSR 39 (1943) 11.
- 717 [48] B.M. Deryagin, S.M. Levi, Film Coating Theory, The Focal Press, New York, 1964.
- 718 [49] D.A. White, J.A. Tallmadge, A gravity corrected theory for cylinder withdrawal,
- 719 Aiche J. 13(4) (1967) 745-+.
- 720 [50] S.D.R. Wilson, The drag-out problem in film coating theory, Journal of
- 721 Engineering Mathematics 16(3) (1982) 209-221.
- 722 [51] S.D.R. Wilson, Coating flow on to rods and wires, Aiche J. 34(10) (1988) 1732-
- 723 1735.
- 724 [52] J. Eggers, Nonlinear dynamics and breakup of free-surface flows, Rev. Mod. Phys.
- 725 69(3) (1997) 865-929.
- 726 [53] G.K. Batchelor, An introduction to fluid dynamics, Cambridge University Press,
- 727 New York, 2000.
- 728 [54] C. Huh, L.E. Scriven, Shapes of axisymmetric fluid interfaces of unbounded extent,
- 729 Journal of Colloid and Interface Science 30(3) (1969) 323-337.
- 730 [55] B. Jin, A. Acrivos, A. Munch, The drag-out problem in film coating, Physics of
- 731 Fluids 17(10) (2005) 12.
- 732 [56] O. Kim, J. Nam, Confinement effects in dip coating, Journal of Fluid Mechanics 827
- 733 (2017) 1-30.

- 734 [57] D.M. Campana, S. Ubal, M.D. Giavedoni, F.A. Saita, Dip Coating of Fibers in the
- 735 Visco-inertial Regime: Numerical Analysis, Industrial & Engineering Chemistry
- 736 Research 52(35) (2013) 12646-12653.
- 737 [58] M. Jenny, M. Souhar, Numerical simulation of a film coating flow at low capillary
- 738 numbers, Computers & Fluids 38(9) (2009) 1823-1832.
- 739 [59] K.G. Kornev, P.H. Adler, Physical determinants of fluid feeding in insects, in: H.
- 740 Krenn (Ed.), Insect mouthparts- form, function, development and performance,
- 741 Springer, New York, 2019, pp. 263-314.